

Band-Limited Signal Reconstruction From Irregular Samples With Variable Apertures

David G. Long, *Fellow, IEEE*, and Reinhard O. W. Franz

Abstract—Sampling plays a critical role in remote sensing and signal analysis. In conventional sampling theory, the signal is sampled at a uniform rate at a minimum of twice the signal bandwidth. Sampling with an aperture function requires a fixed-aperture function, which can be removed by deconvolution after signal reconstruction. However, in some cases, the signal samples are available only at irregular positions, and different samples use different aperture functions. In this paper, the theory of finite-length signal reconstruction with irregular samples and variable apertures in one and two dimensions is considered. In the 1-D case, a band-limited discrete signal can be exactly reconstructed from a finite number of arbitrarily spaced samples with few restrictions on the aperture functions. Exact reconstruction in the 2-D case requires the sampling matrix be invertible, and is not always possible. Variable aperture functions, while complicating the process, can enable reconstruction for a broader range of sample locations. Practical issues are discussed, and numerical examples are provided. Variable aperture reconstruction has application in a variety of remote sensing problems. In this paper, reconstruction from 2-D irregular sampling with variable apertures is illustrated using Special Sensor Microwave/Imager radiometer observations.

Index Terms—Aperture function, irregular samples, point-spread function, reconstruction, sampling, variable aperture.

I. INTRODUCTION

RECONSTRUCTION of sampled signals is a common activity in remote sensing. In a typical remote sensing application, observations (measurements) are samples of an aperture-filtered signal. The aperture results from spatial filtering characteristics of the antenna, optics, and/or signal processing used in the signal sampling. Signal sampling may involve a combination of platform movement, scanning, and pulsed operation, among others. The signal and sampling are frequently two dimensional. From the set of samples, we desire to reconstruct the original signal over the sampling area.

Reconstruction of a band-limited signal from uniformly spaced samples is a well-understood problem treated in standard signal processing textbooks (e.g., [1]): given uniformly spaced samples of the signal, the original band-limited signal can be exactly reconstructed from the samples by sinc inter-

polation¹ so long as the signal is sampled at twice the highest frequency of the signal, i.e., as long as the sampling meets the Nyquist criterion. Uniform spacing of the samples is also known as “regular sampling.” We note that this traditional band-limited reconstruction relies on infinite samples, which cannot be practically collected, thus more general reconstruction techniques should be used [2]. Approximate solutions based on oversampling and filtering or interpolation are commonly used.²

When the signal is sampled with a fixed aperture function,³ the original signal can be recovered from the samples by deconvolution of the aperture function and an intermediate signal resulting from reconstruction from the samples assuming no aperture function.⁴ So long as the spectrum of the aperture function has no nulls in the signal bandwidth, the original signal can be completely recovered. Otherwise, there may be some loss of information.

In some remote sensing applications, only a finite number of measurements are available, and the observations (samples) are not uniformly spaced due to the sensor measurement geometry or platform motion, resulting in irregular (nonuniformly spaced) sampling. Furthermore, the effective aperture may be different for each of the observations, a condition called “variable aperture” sampling. A number of techniques have been published for signal reconstruction from irregular arbitrarily spaced samples, e.g., [2] and [5]–[9] and the references therein; however, the general solution to the problem of signal reconstruction from irregular sampling with variable aperture functions has been only recently developed [10], and the limitations of reconstructability for two dimensions have not been fully addressed.

To make this earlier work more accessible in this paper, we use a tutorial approach to discuss the problem of band-limited signal reconstruction from irregular samples for variable and fixed apertures and present a general discrete signal solution in one and two dimensions. The discrete signal method is chosen since, in practice, the signals of interest are defined only over a bounded domain and only a limited number of samples are available. Novel contributions of this paper include a discussion of practical considerations, a presentation of the sampling limitations in 2-D reconstruction from the irregular sampling, an

Manuscript received July 24, 2015; revised September 12, 2015; accepted November 11, 2015. Date of publication December 30, 2015; date of current version March 9, 2016.

D. G. Long is with the Department of Electrical and Computer Engineering, Brigham Young University, Provo, UT 84602 USA (e-mail: long@ee.byu.edu).

R. O. W. Franz is with the Ira A. Fulton College of Engineering and Technology, Brigham Young University, Provo, UT 84602 USA (e-mail: franz@et.byu.edu).

Color versions of one or more of the figures in this paper are available online at <http://ieeexplore.ieee.org>.

Digital Object Identifier 10.1109/TGRS.2015.2501366

¹Sinc interpolation is equivalent to low-pass filtering of a zeroth-order-hold signal.

²An example is interferometric synthetic aperture radar data analysis for which window-based interpolation schemes have been developed [3], [4].

³An aperture function is also called a point-spread function, a spatial response function, or an impulse response function.

⁴This is equivalent to assuming an ideal delta function aperture function.

empirical analysis of the ratio of sample density and bandwidth, and a derivation of the general matrix formulation for irregular sampling with variable apertures. To illustrate the technique, simulation results are presented for a realistic sensor.

This paper is organized as follows: after background and discussion, using a matrix approach, we show that a band-limited 1-D signal can be reconstructed from arbitrarily located samples. We then extend the derivation to the case of variable apertures. We then consider 2-D signals, which require some constraints on the locations of the irregular samples to ensure full reconstruction. An illustrative example is provided demonstrating the utility of the technique in remote sensing based on reconstruction of brightness temperature images from spaceborne radiometer data.

A. Background

Here, we discuss classic reconstruction theory for continuous-time signals, the connection between continuous-time and discrete-time signals, and the reconstruction of discrete-time signals from ideal and aperture-filtered uniformly spaced samples.

Consider two fundamental ideas in signal analysis: the periodicity assumption implied by discrete sampling of a band-limited finite-length signal and discrete subsampling. We note that all practical signals are bounded.

When teaching introductory signal processing, it is common to assume infinite-length continuous signals (e.g., $f(t) = \sin t$). In analyzing ideal 1-D signal reconstruction from samples, a continuous band-limited signal $f(t)$ is uniformly sampled at an interval of T with an infinite number of samples. The ideally sampled signal is written as $f[n] = f(nT)$, where $f[n]$ is a discrete-time signal, with n being an integer. Assuming that $1/T$ is greater than twice the highest frequency present in $f(t)$ (often called the ‘‘Nyquist sample rate’’), the Shannon–Wittaker–Kotelnikov sampling theorem (see [1]) assures us that $f(t)$ can be reconstructed from $f[n]$ using

$$f(t) = \sum_{n=-\infty}^{\infty} f[n] \operatorname{sinc} \left(\frac{(t - nT)}{T} \right) \quad (1)$$

where $\operatorname{sinc}(x) = \sin(\pi x)/\pi x$.

In practice, however, we can only observe a signal over a finite domain with a finite number of samples. Unless the form of the underlying signal is known analytically, an arbitrary signal cannot generally be fully reconstructed from only a finite number of samples. We recall that, when sampling a signal, there is an *implicit assumption that the signal is band limited*; otherwise, aliasing and loss of signal information occur in representing the signal from its samples [1].

Recalling that a finite-length signal can be made periodic by extension, we note that, in order for a signal to be consistently represented by a finite number of samples and be simultaneously band limited, we must assume the signal to be periodic. In effect, finite sampling and reconstruction implicitly require that we treat the signal as both periodic and band limited in order to consistently interpret sampling and reconstruction. We note that a bounded continuous band-limited periodic signal can be always exactly represented by a discrete-time signal [1], [10].

With these preliminaries, we observe that the sampling of a band-limited continuous signal can be viewed as equivalent to subsampling a discrete-time signal corresponding to the original signal. To explore this for a 1-D signal, denote the signal of interest by $f(t)$. Suppose there are R samples of $f(t)$ available at the arbitrary sample points $t = t_j$ for $j = \{1 \dots R\}$. Real-world considerations suggest that the spacings of the sample points have a rational relationship. Thus, t_j can be written as

$$t_j = n_j T + T_0 \quad (2)$$

where n_j is an integer, T_0 is a real constant, and T is some interval for which (2) holds for all j . In general, there are an infinite number of possible T values.⁵ We prefer to choose the largest T subject to $1/T > 2B$, where B is the highest frequency present in the band-limited $f(t)$. This T is hereafter referred to as the high-rate sample interval (HSI).

Based on the earlier discussion, since the signal $f(t)$ is band limited, it can be exactly represented by its discrete-time counterpart $f[n] = f(nT)$, where T is the HSI. Thus, for practical signal reconstruction, we need only reconstruct $f[n]$ from the samples $f[n_j]$. The signal $f(t)$ can be reconstructed from $f[n]$ using (1), where the infinite sum in (1) is computed modulo of the period so that only one period of the values of $f[n]$ is required.

Thus, the sampling of the continuous signal $f(t)$ is equivalent to the discrete sampling of the discrete signal $f[n]$. The available samples extend over the finite domain defined by NT , where T is the HSI, and N is the (assumed) signal period. The period count N may be larger than $\max(n_j) - \min(n_j)$, but if smaller, the indices n_j are mapped to $n \in \{0, \dots, N - 1\}$. Without information about the signal structure, selection of N in practice can be arbitrary and requires engineering judgment.

The discrete Fourier transform (DFT) $F[k]$ of $f[n]$ can be written as

$$F[k] = \sum_{j=0}^{N-1} f[j] W_N^{kj} \quad (3)$$

where $W_N^{kj} = e^{-i2\pi kj/N}$, and $i = \sqrt{-1}$ [1]. Since $f[n]$ is band limited to B , $F[k] = 0$ for all $|k| > M$, where $M \leq NB/2T$, and the discrete signal $f[n]$ is called M -band-limited. Note that $F[k]$ approximates the continuous Fourier transform $F(\omega)$ of the underlying continuous $f(t)$ for $\omega < \pi M/NT$ [1].

In the 1-D case, the M -band-limited discrete signal $f[n]$ can be perfectly reconstructed from the irregular samples $f[n_j]$ for arbitrary n_j , so long as the $R \geq 2M + 1$ samples $n_j \bmod N$ are distinct [8]. Additional samples can reduce the effects of noise in noisy processes [5], [6]. Efficient numerical algorithms for irregular reconstruction have been developed [6].

As will be discussed later, unlike 1-D reconstruction, 2-D reconstruction is not always possible for arbitrarily located samples. Accurate 2-D reconstruction imposes restrictions on the sample locations.

⁵This is readily seen by noting that if a particular value of T satisfies (2) for all j , the value d where $T = md$ for an arbitrary integer $m > 0$ also satisfies (2).

The sampling discussed so far assumes an ideal aperture function where the observation of the signal $f[n]$ at n_j is $f[n_j]$. Practical aperture functions result in observation values that are locally averaged and weighted values of the signal. Local averages smaller than the maximum sample spacing are treated by [11]; however, as discussed in the following, larger apertures can be used. In general, the observation values can be modeled as ideal samples of the aperture-filtered signal. For example, in one dimension using the discrete signal model with the aperture function $v[n]$, the observation sample is $g[n_j]$, where g is the aperture-filtered signal given by $g[n] = v[n] * f[n]$, where $*$ denotes discrete convolution. For the fixed-aperture case, the samples can be first used to reconstruct $g[n]$ from the observations; then, signal deconvolution techniques can be used to compute $f[n]$ from $g[n]$. So long as the aperture spectrum does not have any nulls over the bandwidth of the signal spectrum, the signal can be reconstructed perfectly. However, when different apertures are used for different samples—a common case in remote sensing—the deconvolution approach cannot be used. In the following, we show how fixed or variable aperture functions can be incorporated into the reconstruction process to directly estimate the original signal.

II. ONE-DIMENSIONAL SAMPLING AND RECONSTRUCTION

This section considers 1-D reconstruction. To simplify the development, we first consider uniform or regular sample reconstruction and then irregular sampling and reconstruction without an aperture function. Finally, the general case of irregular sampling with a variable aperture is considered.

A. Preliminaries

In discrete signal processing with periodic signals, the Dirichlet kernel plays an analogous role with the sinc function in continuous signal processing. The discrete Dirichlet kernel can be written as

$$D_{M,N}(n) = \sum_{k=-M}^M W_N^{-kn} \quad (4)$$

$$= \begin{cases} \frac{\sin(\frac{(2M+1)\pi n}{N})}{\sin(\frac{\pi n}{N})}, & n \neq 0 \\ 2M+1, & \text{else} \end{cases} \quad (5)$$

which is periodic in n with period $N > 0$ and is M -band-limited. An illustrative plot of $D_{M,N}(n)$ for a particular M and N is shown in Fig. 1.

Since

$$\begin{aligned} & \langle D_{M,N}(n-n_i), D_{M,N}(n-n_j) \rangle \\ &= \sum_{i=0}^{N-1} \sum_{j=0}^{N-1} D_{M,N}(n-n_i) D_{M,N}(n-n_j) \\ &= N D_{M,N}(n_i-n_j) \end{aligned} \quad (6)$$

it follows that $D_{M,N}(n-n_i)$ and $D_{M,N}(n-n_j)$ are orthogonal if and only if $(n_i-n_j)(2M+1) = n'N$ for some integer

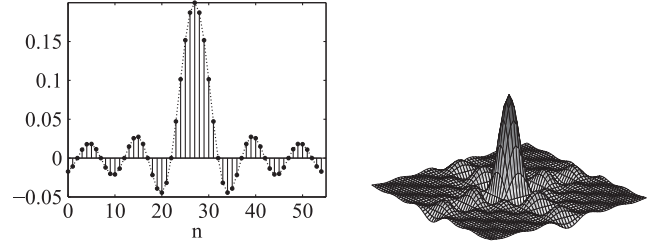


Fig. 1. Examples of (left) 1-D [$N = 55$, $M = 5$] and (right) 2-D [$N_1 = N_2 = 55$, $M_1 = M_2 = 5$] Dirichlet kernels. One period of each kernel is shown.

$n' \neq 0$. The set of vectors generated by $D_{M,N}(n-jd); j = 0, 1, \dots, 2M$ for integer $d = N/(2M+1)$ forms an orthogonal basis for the space of all discrete band-limited functions of period N .⁶ Thus, any discrete M -band-limited function with period N can be expressed as

$$f[n] = \sum_{j=0}^{2M} a_j D_{M,N}(n-jd) \quad (7)$$

with $f[n+kN] = f[n]$ for all integer k . This is the discrete equivalent of (1) when $a_j = (d/N)f[jd]$ and corresponds to interpolation by the Dirichlet kernel. Note that, by construction, $f[n]$ is M -band-limited and periodic with period N .

Equation (7) can be formulated as the matrix equation

$$\mathbf{f} = \mathbf{D}\mathbf{a} \quad (8)$$

where the N element signal vector \mathbf{f} has elements $(\mathbf{f})_n = f[n]$, \mathbf{a} has $2M+1$ elements a_j , and the $N \times (2M+1)$ matrix \mathbf{D} has elements

$$(\mathbf{D})_{k,l} = D_{M,N}(k-l d). \quad (9)$$

Equation (8) is the matrix formulation of the regular reconstruction equation. As shown later, this result can be generalized to deal with irregularly spaced sampling.

B. Reconstruction From Regular Samples

The regular, or uniform, discrete-time sampling and reconstruction problem can be formulated as follows. Any periodic M -band-limited discrete signal f with period N can be reconstructed exactly from $R \geq 2M+1$ samples $f_s[j]$, where $f_s[j] = f[jd]$, with d being the integer sample spacing and $jd \bmod N$ distinct. Ideally, $R = N/d$.

The regularly sampled signal $f_s[n]$ can be written as

$$\mathbf{f}_s = \mathbf{D}_o \mathbf{a} \quad (10)$$

where \mathbf{D}_o is the $R \times (2M+1)$ matrix constructed from the R rows of \mathbf{D} corresponding to the values $n = jd, j = 0, 1, \dots, R-1$, with \mathbf{f}_s containing $2M+1$ elements $(\mathbf{f}_s)_k = f[kd]$.

⁶Strictly speaking, d does not need to be an integer; however, when d is not an integer, a_j in (8) correspond to Dirichlet-interpolated values of $f[n]$ rather than to specific samples of $f[n]$. Nevertheless, the reconstruction equations [(8), (10), and (11) for regular sampling and (13) and (15) for irregular sampling] can be applied for noninteger d .

Given \mathbf{f}_s , we want to compute \mathbf{a} . In order to compute the $2M + 1$ values in \mathbf{a} necessary to fully reconstruct the signal, it is sufficient to show that the inverse of \mathbf{D}_\circ exists. Then

$$\mathbf{a} = \mathbf{D}_\circ^{-1}\mathbf{f}_s. \tag{11}$$

\mathbf{a} can be then used to reconstruct the signal using the reconstruction equation, i.e., (8).

For the regular sampling case with $R = 2M + 1$, the elements of the matrix $\mathbf{D}_\circ = \mathbf{D}$ can be written explicitly as

$$(\mathbf{D}_\circ)_{l,m} = D_{M,N}(ld - md) = \sum_{k=-M}^M W_N^{-kld} W_N^{kmd}. \tag{12}$$

As demonstrated in the Appendix, the \mathbf{D}_\circ matrix is always invertible so that (11) can be used to compute \mathbf{a} , which can be then used to reconstruct the signal using the discrete sampling equation $\mathbf{f} = \mathbf{D}\mathbf{a}$. We note that, for the regular sampling reconstruction case with $d(2M + 1) = N$, \mathbf{D}_\circ [d integer] is, in fact, a scaled identity matrix so that $\mathbf{a} = (d/N)\mathbf{f}_s$.

When the signal is oversampled, i.e., there are more than the minimum required $2M + 1$ signal samples available, the matrix \mathbf{D}_\circ is rectangular, but still has full column rank. In this case, the Moore–Penrose pseudoinverse can be used in place of the conventional inverse in (11), resulting in a unique estimate of \mathbf{a} . If there is no noise in the problem, the solution for \mathbf{a} is precisely the same for all $N \geq R \geq (2M + 1)$. A longer discussion on oversampling is provided in the next section.

C. Reconstruction From Irregular Samples

The previous derivation can be extended to the case of sampling a signal at irregular intervals. The $R = 2M + 1$ irregular samples \mathbf{f}_{is} can be represented in matrix form as

$$\mathbf{f}_{is} = \mathbf{D}_\Delta \mathbf{a} \tag{13}$$

where \mathbf{D}_Δ is the $R \times (2M + 1)$ matrix constructed from the R rows of \mathbf{D} corresponding to the distinct sample points $n_l \in \{0, \dots, N - 1\}$, $l = 1, 2, \dots, R$, with \mathbf{f}_{is} having the R elements $(\mathbf{f}_{is})_l = f[n_l]$. The elements of the matrix \mathbf{D}_Δ can be written explicitly as

$$\begin{aligned} (\mathbf{D}_\Delta)_{l,m} &= D_{M,N}(n_l - md) \\ &= \sum_{k=-M}^M W_N^{-kn_l} W_N^{kmd}. \end{aligned} \tag{14}$$

In order to compute the $2M + 1$ values of \mathbf{a} necessary to fully reconstruct the signal [using (8)], \mathbf{D}_Δ^{-1} must exist. This is shown in the Appendix for arbitrary disjoint n_j .

While it is possible to write \mathbf{D}_Δ^{-1} in closed form, the closed-form inverse is impractical for numerical computation. Instead, well-known conventional numerical inverse methods can be used to compute \mathbf{D}_Δ^{-1} or solve the corresponding linear system. We point out that \mathbf{D}_Δ and \mathbf{D}_Δ^{-1} depend only on the sample locations and not on the sample values. Thus, if the sample

locations remain the same, multiple reconstructions can be accomplished with only one matrix inversion. Fast numerical methods for solving (13) are considered in [6].

Since \mathbf{D}_Δ^{-1} exists, it is possible (at least theoretically) to compute

$$\mathbf{a} = \mathbf{D}_\Delta^{-1}\mathbf{f}_{is} \tag{15}$$

no matter what the precise values of n_j are, so long as they are distinct. Once \mathbf{a} is computed, it can be then used to reconstruct the signal using the discrete sampling equation, i.e., (8). Reconstruction from irregular samples can be thus viewed as a two-step process: first, compute the frequency coefficients of the signal using (15), and then, reconstruct the full signal using (8).

We point out that, once \mathbf{a} is computed from the locations of the irregular samples, the reconstruction of $f[n]$ is independent of the original sample locations. Furthermore, when there is no sampling noise, \mathbf{a} computed from either irregular or regular sampling is identical. Some computation can be saved if the reconstructed signal is only needed at particular locations. In this case, \mathbf{a} is first computed from the samples. Then, the forward reconstruction equation, i.e., (8), can be used with \mathbf{D} containing only the rows corresponding to the desired locations.

In the oversampled case where $R > 2M + 1$, \mathbf{D}_Δ is rectangular, but remains full column rank. It is overdetermined and therefore has a unique pseudoinverse. While the “extra” samples could be discarded to make \mathbf{D}_Δ square, retaining all of the samples improves the performance in the presence of sampling noise [6]. When $R > 2M + 1$, the pseudoinverse is used in (15) to compute \mathbf{a} . We note that, in the noise-free case, the same \mathbf{a} results no matter the number (subject to $R \geq 2M + 1$) or the locations of the samples so long as they are distinct.

D. Variable Apertures

The previous section showed that a 1-D discrete periodic M -band-limited signal can be reconstructed from $2M + 1$ arbitrary irregular samples. There is no restriction on where the sample points are located—only that they are distinct. This result has been derived previously [8]. However, the variable-aperture case has not been previously considered. Here, we consider the variable-aperture case.

As noted, in practice, the observed signal is frequently filtered through an aperture or a point-spread function prior to sampling. Such may arise due to the response function of an antenna, lens, or other signal processing. In general, the aperture may be different for each observation. While the effects of a single fixed aperture function can be removed by deconvolution, handling variable apertures requires a more general approach.

Let $v_j[n]$ be the aperture corresponding to the j th observation. Effectively, v_j is the impulse response of the aperture. Typically, the aperture is like a window with a central peak centered at the sample location and has a finite length. The aperture is generally much shorter than the signal, and thus has a wider bandwidth of support. Define the j th aperture-filtered

signal as $f_j[n] = v_j[n] * f[n]$. Note that $f_j[n]$ is band limited to the minimum band limit of the signal $f[n]$ or aperture function $v_j[n]$.⁷ The j th sampled observation is $g_j = f_j[n_j]$.

Assuming $v_j[n]$ is reasonably well behaved, we can write

$$f_j[n] = v_j[n] * f[n] = \sum_{k=0}^{N-1} f[k]v_j[n-k] \quad (16)$$

where v_j is treated as periodic modulo N so that the observation samples $g_j = f_j[n_j]$ are

$$g_j = (v_j[n] * f[n])|_{n=n_j} \quad (17)$$

$$= \sum_{k=0}^{N-1} f[k]v_j[n_j - k]. \quad (18)$$

Using (7), the sample g_j can be written as

$$g_j = \sum_{k=0}^{N-1} \sum_{l=0}^{2M} a_l D_{M,N}(k - ld)v_j[n_j - k] \quad (19)$$

$$= \sum_{l=0}^{2M} a_l H_j(n_j; l) \quad (20)$$

where $H_j(n_j; l)$ is defined as the convolution of the Dirichlet kernel $D_{M,N}(n - ld)$ and the aperture function $v_j[n]$ sampled at n_j , i.e.,

$$H_j(n_j; l) = [v_j[n] * D_{M,N}(n - ld)]|_{n=n_j}. \quad (21)$$

In matrix form, the variable aperture sampling equation is

$$\mathbf{g} = \mathbf{D}_v \mathbf{a} \quad (22)$$

where $(\mathbf{g})_j = g_j[n_j]$, and \mathbf{D}_v is the $R \times (2M + 1)$ sampling matrix whose rows are $H_j(n_j; l)$ for $l = 0, \dots, 2M$. Explicitly

$$\begin{aligned} (\mathbf{D}_v)_{j,l} &= H_j(n_j; l) \\ &= \sum_{k=0}^{N-1} v_j[n_j - k] D_{M,N}(k - ld) \end{aligned} \quad (23)$$

$$= \sum_{k=0}^{N-1} v_j[n_j - k] \sum_{m=-M}^M W_N^{-m(k-ld)} \quad (24)$$

$$= \sum_{k=0}^{N-1} v_j[n_j - k] \sum_{m=-M}^M W_N^{-mk} W_N^{mld}. \quad (25)$$

Given the sample values \mathbf{g} , the vector \mathbf{a} can be computed by inverting (22), if the sampling matrix \mathbf{D}_v is invertable.

The matrix \mathbf{D}_v is invertable if and only if the columns of \mathbf{D}_v are linearly independent, which depends on the relationship of the aperture functions as shifted to the sampling location. In the ideal aperture case, $v_j[n] = \delta[n - n_j]$, so that $\mathbf{D}_v = \mathbf{D}_\Delta$.

Fortunately, most practical apertures tend to be well behaved. These include finite-length window-like apertures centered at the (distinct) sample locations.⁸ In these cases, the matrix \mathbf{D}_v is invertable. Notably, a fixed aperture ($v_j[n] = v[n - n_j]$), where $v[n]$ is well behaved, such as a window function, ensures invertability.

If \mathbf{D}_v is full column rank, the value of \mathbf{a} computed from the variable aperture samples is unique and permits reconstruction of $f[n]$ using (8) for any set of distinct sample locations (subject to $R \geq 2M + 1$) and apertures. When extra samples are available, the pseudoinverse can be used. In the noise-free case, the result is precisely the same values for \mathbf{a} as when the minimum number of distinct samples is used.

E. Computational Considerations

In the previous sections, it is shown that, regardless of where the signal is sampled, the resulting \mathbf{D}_Δ matrix is invertable, enabling reconstruction of the periodic band-limited signal $f[n]$ given any $2M + 1$ samples within the period. The samples could, in fact, be adjacent. However, the sample locations do affect the computation of the inverse of the \mathbf{D}_Δ or \mathbf{D}_v matrices as quantified by the condition number of the matrices. The condition number κ is the ratio of the largest to smallest eigenvalues. A large condition number implies that the inverse is sensitive to numerical computation errors. Thus, poor condition numbers can limit the practical implementation of the approach, although the matrix is known to be invertable. We note that the condition number is a function only of the sample locations and aperture function, and not of the signal values.

As we have seen, reconstruction of the sampled signal involves the solution of the linear system given by (13) for the case of no aperture (which is equivalent to an ideal δ function aperture) or (22) for the aperture-filtered case. This can be computationally taxing, particularly for large R . When using no aperture, the active weights conjugate gradient Toeplitz method (ACT algorithm) [6] is a computationally efficient method for solving the system for 1-D reconstruction from irregular samples. The ACT method can be extended to a single fixed aperture by first reconstructing the aperture-filtered signal from the samples and then deconvolving the aperture function and signal. However, the ACT algorithm does not support variable apertures.

For the variable-aperture case, a numerical approach must be used. Fortunately, numerical methods permit solutions of very large order even when the condition number is quite large. Values of R in hundreds or more are practical, and large values can be used with very high precision computation. While there are so many variations that it is difficult to generalize the effects of the variable aperture, we have found that most practical apertures tend to regularize \mathbf{D}_Δ , reducing the condition number relative to an ideal [δ function] aperture. Occasionally, for particularly poor sampling distributions, the apertures can degrade the condition number compared with an ideal aperture. While poorly behaved apertures can produce noninvertable \mathbf{D}_v

⁷Here, we assume that none of the apertures has frequency nulls in the signal bandwidth.

⁸An example of a poorly behaved aperture is $v_j[n] = 1$, which results in a noninvertable \mathbf{D}_v .

matrices, in the authors' experience, poorly behaved apertures are rarely encountered in practice.

Iterative approaches to matrix inversion or linear system solution can be very effective for reconstruction, and iterative methods are commonly used to refine matrix inverses computed using QR factorization or other methods. We note that iterative methods can be also used to compute approximate reconstructions. These are particularly useful for very large problems with thousands or millions of samples. Examples of iterative reconstruction methods include algebraic reconstruction methods (e.g., [12]) and the scatterometer image reconstruction (SIR) method [13]. Although SIR was not originally explicitly formulated as a discrete reconstruction method, the linear form of SIR is an iterative approximation of the reconstruction method described here. Other variations are possible, e.g., [14].

III. TWO-DIMENSIONAL SAMPLING AND RECONSTRUCTION

Extending the 1-D results to higher dimensions seems straightforward. However, unlike in the 1-D case where the only requirements on the sample locations are that they be distinct, in the 2-D sampling case, there are some sampling distributions that do not enable 2-D reconstruction. For example, if all the samples are in a straight line, they are effectively single dimensional, and general 2-D reconstruction is not possible.⁹ On the other hand, for 2-D signals band limited to rectangular spectrum of support, sampling using a generalized "cubic lattice" location scheme (defined later) is always fully reconstructable, even if the lattice spacing is nonuniform. While general 2-D sample location requirements that enable full reconstruction of band-limited signals are difficult to simply state, a given sampling configuration can be tested by evaluating the rank of the 2-D reconstruction matrix described later.

A. Preliminaries

Following the 1-D case, a discrete 2-D signal $f[n_1, n_2]$ with 2-D period $[N_1, N_2]$ is considered that is $[M_1, M_2]$ -band-limited, i.e., the signal has a rectangular region of support in the frequency domain.¹⁰ Thus, its 2-D DFT $F[k_1, k_2]$ can be written as [compare (3)]

$$F[k_1, k_2] = \sum_{n_1=0}^{N_1-1} \sum_{n_2=0}^{N_2-1} f[n_1, n_2] W_{N_1}^{k_1 n_1} W_{N_2}^{k_2 n_2}. \quad (26)$$

Since $F[k_1, k_2]$ is $[N_1, N_2]$ -periodic, we need only consider a single period in the following discussion.

For convenience, the 2-D signal is expressed as a row-major ordered vector, although any consistent ordering could be used. Over a $[N_1, N_2]$ period, $f[n_1, n_2]$ is written in row-major ordering as the $N_1 N_2$ length vector \mathbf{f} with elements $(\mathbf{f})_j = f[n_1, n_2]$, where $j = n_2 N_1 + n_1$, with $n_1 \in \{0, 1, \dots, N_1\}$

⁹Other examples of nonreconstructable sample distributions can be generated (see Fig. 2).

¹⁰Other definitions of 2-D band limit exist that couple the coordinates. These have different sampling requirements [2], [15]. This paper considers only a rectangular region of support to define the band limit.

and $n_2 \in \{0, 1, \dots, N_2\}$. To illustrate the ordering, the 2-D locations

$$\begin{bmatrix} (0, 0) & (0, 1) & \cdots & (0, N_2 - 1) \\ (1, 0) & (1, 1) & \cdots & (1, N_2 - 1) \\ \vdots & \vdots & \ddots & \vdots \\ (N_1 - 1, 0) & (N_1 - 1, 1) & \cdots & (N_1 - 1, N_2 - 1) \end{bmatrix}$$

become the 1-D vector

$$\begin{bmatrix} (0, 0) \\ (1, 0) \\ (2, 0) \\ \vdots \\ (N_1 - 1, 0) \\ (0, 1) \\ (1, 1) \\ \vdots \\ (N_1 - 1, 1) \\ (0, 3) \\ (1, 2) \\ \vdots \\ (N_1 - 1, N_2 - 1) \end{bmatrix}.$$

Equation (26) defines a rectangular region of support in the frequency domain where $F[k_1, k_2] = 0$ for $|k_1| > M_1$ or $|k_2| > M_2$. Note that there are only R , where $R = R_1 R_2$ with $R_1 = 2M_1 + 1$ and $R_2 = 2M_2 + 1$, nonzero entries in $F[k_1, k_2]$. Thus, the minimum number of samples required to fully reconstruct an arbitrary $[M_1, M_2]$ -band-limited signal is R .

In conventional sampling theory, the samples are required to be located on a regular (uniformly spaced) 2-D grid (known as a "uniform cubic lattice", e.g., the $n_{i,j}$ th sample is at $[i d_1, j d_2]$, where $d_1 = N_1 / (2M_1 + 1)$, and $d_2 = N_2 / (2M_2 + 1)$ [d_1 and d_2 integers]).¹¹ Such a sampling is a specific example of the more general "generalized cubic lattice" sampling scheme defined as the cross product of two 1-D samplings, one along each dimension [15].

Consider R_1 distinct sample indexes $(n_1)_i \in \{0, \dots, N_1 - 1\}$ and R_2 distinct indexes $(n_2)_j \in \{0, \dots, N_2 - 1\}$. The sampling location sets $\{(n_1)_i\}$ and $\{(n_2)_j\}$ are called the "marginal samplings." A gridded cubic lattice sampling consists of $R = R_1 R_2$ samples located at $n_{i,j} = [(n_1)_i, (n_2)_j]$.

In contrast to generalized cubic sampling, general 2-D sampling has R distinct samples arbitrarily located within a spatial period, with no structure required. Fig. 2 illustrates examples of these different 2-D sampling schemes.

B. Two-Dimensional Reconstruction

Here, it is shown that cubic lattice sampling can be a sufficient condition for full reconstruction; however, it is

¹¹As in the 1-D case, nonintegers d_1 and d_2 can be used; however, as in the 1-D case, for simplicity, in this paper, we assume integer values for d_1 and d_2 . Thus, N_1 and N_2 are integer multiples $2M_1 + 1$ and $2M_2 + 1$, respectively.

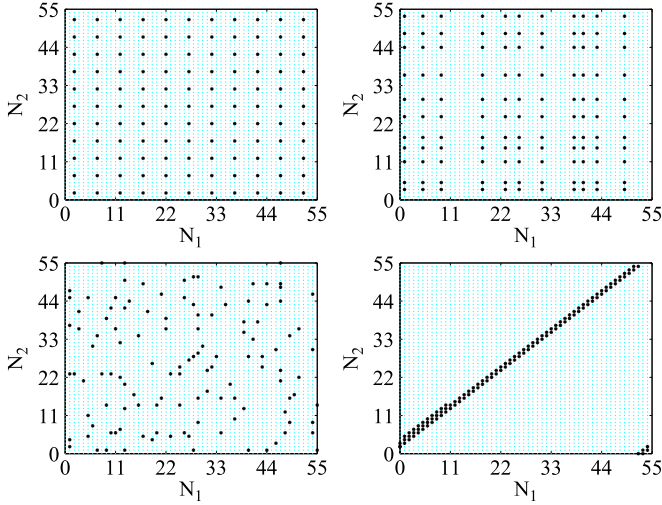


Fig. 2. Examples of 2-D sampling for $[N_1 = N_2 = 45, M_1 = M_2 = 5]$. (Upper left) Uniform cubic lattice. (Upper right) Irregular cubic lattice. (Lower left) General reconstructable. (Lower right) Nonreconstructable.

not a necessary condition for general $[M_1, M_2]$ -band-limited reconstruction—many other general sampling configurations are possible. A method for evaluating these more general cases is derived. Unlike the 1-D case, merely having R disjoint samples is not sufficient to ensure full reconstruction—the sampling must be full rank.

The condition expressed in (26) means that an arbitrary $[M_1, M_2]$ -band-limited discrete 2-D signal $f[n, m]$ can be written as

$$f[n_1, n_2] = \sum_{p_1=0}^{2M_1} \sum_{p_2=0}^{2M_2} a_{p_1, p_2} D_{M_1, N_1}(n_1 - p_1 d_1) \times D_{M_2, N_2}(n_2 - p_2 d_2) \quad (27)$$

which is the 2-D equivalent of (7), where the 2-D Dirichlet kernel is formed from the product of two 1-D Dirichlet kernels (see Fig. 1).

In matrix–vector notation, the row-major ordered 2-D equivalent to (8) is

$$\mathbf{f} = \mathcal{D} \mathbf{a} \quad (28)$$

where \mathbf{a} is an $R = R_1 R_2$ vector with $(\mathbf{a})_l = a[p_1, p_2]$, $p = p_2 R_1 + p_1$, and \mathcal{D} is an $(N_1 N_2) \times R$ element matrix of sampled Dirichlet kernels, where

$$(\mathcal{D})_{k, l} = D_{M_1, N_1}(n_1 - p_1 d_1) D_{M_2, N_2}(n_2 - p_2 d_2) \quad (29)$$

with $k = n_2 N_1 + n_1$ and $l = p_2 R_1 + p_1$. Thus, \mathcal{D} has a block form that can be constructed from two \mathbf{D} matrices [see (9)] using the appropriate M and N values, e.g., \mathcal{D} can be expressed as the Kronecker or direct product of the \mathbf{D} matrices along each axis, i.e.,

$$\mathcal{D} = \mathbf{D}_{(1)} \otimes \mathbf{D}_{(2)} \quad (30)$$

where \otimes is the Kronecker product¹²; and $\mathbf{D}_{(1)}$ and $\mathbf{D}_{(2)}$ are \mathbf{D} matrices constructed using M_1, N_1 and M_2, N_2 , respectively. Recalling the 1-D development, we note that \mathbf{a} corresponds to an equivalent uniformly spaced regular cubic lattice sampling of f , i.e., for integers d_1 and d_2 , $\mathbf{a} = (d_1 d_2 / N_1 N_2) \mathbf{f}_u$, where $(\mathbf{f}_u)_l = f[p_1 d_1, p_2 d_2]$.

Let $\{S_k\}$ be the set of $R_s \geq R$ distinct sample locations where $S_k = [(n_1)_k, (n_2)_k]$, with $0 \leq (n_1)_k < N_1$ and $0 \leq (n_2)_k < N_2$ arbitrary. The sampled signal vector \mathbf{f}_s has elements $(\mathbf{f}_s)_k = f[S_k] = f[(n_1)_k, (n_2)_k]$ and can be written as

$$\mathbf{f}_s = \mathcal{D}_\Delta \mathbf{a} \quad (31)$$

where the $R_s \times R$ matrix \mathcal{D}_Δ consists of the appropriate rows of \mathcal{D} , i.e., the k th row of \mathcal{D}_Δ is the i th row of \mathcal{D} , where $i = (n_1)_k N_2 + (n_2)_k$. Explicitly

$$\begin{aligned} (\mathcal{D}_\Delta)_{k, l} &= (\mathcal{D})_{i, l} \\ &= D_{M_1, N_1}((n_1)_k - p_1 d_1) D_{M_2, N_2}((n_2)_k - p_2 d_2) \end{aligned} \quad (32)$$

with $i = (n_2)_k N_1 + (n_1)_k$ and $l = p_2 R_1 + p_1$.

From (31), if \mathcal{D}_Δ has full column rank (which, at a minimum, requires $R_s \geq R$), \mathbf{a} can be uniquely computed from \mathbf{f}_s . We note that, when $R_s > R$ and \mathcal{D}_Δ is full column rank, some rows of \mathcal{D}_Δ are linearly dependent on the other rows, which implies that excess rows and their corresponding samples can be eliminated [although extra samples are useful for noise suppression (see Section III-D)]. We are often most interested in the case of critical sampling with $R_s = R$, which has square \mathcal{D}_Δ .

For cubic lattice sampling, it can be shown that

$$\mathcal{D}_\Delta = \mathbf{D}_{\Delta(1)} \otimes \mathbf{D}_{\Delta(2)} \quad (33)$$

where $\mathbf{D}_{\Delta(1)}$ and $\mathbf{D}_{\Delta(2)}$ are 1-D forward sampling matrices defined in (14) for the marginal sampling sets $\{(n_1)_i\}$ and $\{(n_2)_j\}$, respectively. By using the well-known general matrix identity

$$\text{rank}(\mathbf{A} \otimes \mathbf{B}) = \text{rank}(\mathbf{A}) \text{rank}(\mathbf{B}) \quad (34)$$

where \mathbf{A} and \mathbf{B} are arbitrary matrices, and noting that $\mathbf{D}_{\Delta(1)}$ and $\mathbf{D}_{\Delta(2)}$ are full column rank in (33), it follows that \mathcal{D}_Δ is full rank. Thus, for this case, the marginal sampling sets enable full reconstruction of arbitrary 2-D $[M_1, M_2]$ -band-limited signals. This is true for either uniform or irregular marginal sampling schemes. For regular cubic lattice sampling with integers d_1 and d_2 , \mathcal{D}_Δ is a scaled identity matrix, and $\mathbf{a} = (d_1 d_2 / N_1 N_2) \mathbf{f}_s$.

While \mathcal{D}_Δ is always full rank for generalized cubic lattice sampling for more general sampling distributions, \mathcal{D}_Δ is not guaranteed to be full rank, and in fact, exceptions can be found.

¹²The Kronecker product of a $m \times n$ matrix \mathbf{A} and a $p \times q$ matrix \mathbf{B} is a $mp \times nq$ matrix, i.e.,

$$\mathbf{A} \otimes \mathbf{B} = \begin{bmatrix} a_{1,1} \mathbf{B} & \cdots & a_{1,n} \mathbf{B} \\ \vdots & \ddots & \vdots \\ a_{m,1} \mathbf{B} & \cdots & a_{m,n} \mathbf{B} \end{bmatrix}$$

Despite extensive effort on our part, we have been unable to come up with simple description of the requirements for general sampling to ensure full-rank \mathcal{D}_Δ ; however, numerical methods can be used to test the rank of \mathcal{D}_Δ for any particular sampling to ensure invertability. This is discussed further in Section III-D. Note that the rank of \mathcal{D}_Δ is dependent only on the sample locations and not on the sample values.

As in the 1-D case, reconstruction of the 2-D signal f from irregular samples can be viewed as a two-step process. First, the equivalent regular sampling representation \mathbf{a} is computed from the irregular samples by solving (31), which is possible if \mathcal{D}_Δ is full rank. The reconstructed signal is then computed using (28). Note that if the reconstructed signal is only needed at particular locations, \mathbf{a} can be first computed. Then, f can be computed at the desired locations using the appropriate rows of \mathcal{D} in (28) [see (31)].

C. Variable Apertures

As in the 1-D case, the effects of a single constant aperture function for 2-D sampling can be removed by deconvolution; however, a more general approach is required when different apertures are used with different samples.

Let $v_k[n_1, n_2]$ be the effective aperture corresponding to the k th observation. The sample value g_k is the 2-D convolution of the original signal and the aperture function, evaluated at the sample location, i.e.,

$$g_k = (v_k[n_1, n_2] * f[n_1, n_2])|_{S_k} \\ = \sum_{m_1} \sum_{m_2} f[m_1, m_2] v_k [(n_1)_k - m_1, (n_2)_k - m_2] \quad (35)$$

[compare (17) and (18)] where v_k is treated as periodic and the double sum is over the nonzero region of support for v_k , and $S_k = [(n_1)_k, (n_2)_k]$ is the location of the aperture center. Let \mathbf{g} be the R_s element vector of aperture-filtered samples. In matrix form, (35) is

$$\mathbf{g} = \mathbf{D}_g \mathbf{f} = \mathcal{D}_g \mathbf{D} \mathbf{a} = \mathcal{D}_v \mathbf{a} \quad (36)$$

where the rows of \mathcal{D}_g contain the values of v_k to be convolved with the columns of \mathcal{D} . The resulting rows of the $R_s \times R$ element matrix \mathcal{D}_v are aperture-filtered Dirichlet kernels. Explicitly

$$(\mathcal{D}_v)_{k,l} = \sum_{m_1} \sum_{m_2} v_k [(n_1)_k - m_1, (n_2)_k - m_2] \\ \cdot D_{M_1, N_1}(m_1 - p_1 d_1) D_{M_2, N_2}(m_2 - p_2 d_2) \quad (37)$$

$$= \sum_{m_1} \sum_{m_2} v_k [(n_1)_k - m_1, (n_2)_k - m_2] \\ \cdot \sum_{\mu_1=-M_1}^{M_1} \sum_{\mu_2=-M_2}^{M_2} W_{N_1}^{\mu_1 m_1} W_{N_1}^{p_1 d_1} W_{N_2}^{-\mu_2 m_2} W_{N_2}^{p_2 d_2} \quad (38)$$

with $l = p_2 R_2 + p_1$.

By solving (36) with the sample values \mathbf{g} , \mathbf{a} can be computed if the variable aperture sampling matrix \mathcal{D}_v is invertable. If \mathcal{D}_v is not invertable, then \mathbf{a} cannot be precisely computed, and thus, the signal cannot be exactly reconstructed from the samples. In this case, approximate solution methods must be used, e.g., [9] and [13].

The matrix \mathcal{D}_v is invertable if and only if it has full column rank, which depends on the relationship of the apertures as shifted to the sampling location. Including the apertures generally does not change the sampling rank. In numerical experiments described in the following, we have found that the apertures often improve the condition number compared with the ideal aperture matrix, i.e., they tend to regularize the sampling matrix. However, this is not always the case: some aperture functions and samplings do not result in a full-rank \mathcal{D}_v . At present, we do not have a general analytic method for specifying such cases and must rely on numerical tests. We hope to complete a more detailed exploration of the relationship between the variable apertures and the sampling locations in a future paper.

As in the 1-D case, reconstruction of the 2-D signal f from irregular variable aperture samples is a two-step process. Assuming \mathcal{D}_v is full rank, the equivalent regular sampling representation \mathbf{a} is first computed from the irregular samples by solving (36). The reconstructed signal is then computed using (28).

D. Two-Dimensional Sampling Considerations

As previously noted, while cubic lattice sampling can ensure a full-sampling matrix in 2-D sampling, there is no guarantee that an arbitrary 2-D sampling is full rank. To help provide insight into how often an arbitrary 2-D sampling does not result in a full-rank sampling matrix, we conduct a Monte Carlo experiment. For simplicity, we set $M = M_1 = M_2$ and $N = N_1 = N_2$. Two cases for the aperture function were considered: an ideal aperture (a δ function) and a realistic fixed aperture. The latter is a 2-D Hann window of extent M centered at the sample location. The experiment also evaluates the effect of “excess” samples when the number of samples R_s is greater than the minimum number R required for reconstruction.

While cases for small M and d can be reasonably exhaustively tested, this is not practical for larger values; thus, to generate this plot for each case and set of parameters, several thousand different realizations of sets of R_s distinct sample locations were randomly generated. The sample locations were uniformly distributed over the possible locations. For each realization, the rank of the sampling matrix \mathcal{D}_v was numerically determined, and the percentage of full rank matrices was computed. The results are summarized in Fig. 3.

In all cases, this plot shows that the percentage of full-rank 2-D samplings for various values of M and d , where $N = d(2M + 1)$ increases with increasing M . The rate of increase is a function of d , with larger d producing higher full-rank matrix percentages. For $d > 6$, the percentage is almost always 100% for the M values considered. We observe that including the realistic aperture function improves the condition number of

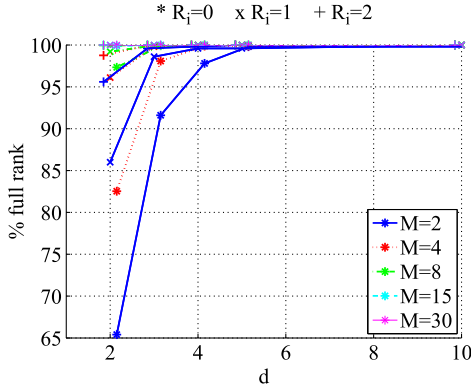


Fig. 3. Numerically computed percentage of random 2-D samplings that produce full-rank reconstruction matrices versus $d_1 = d_2 = d$ for different values of $M_1 = M_2 = M$. R_i indicates the number of additional samples above the minimum R required. In this figure, the line/symbol color is associated with M , whereas the different symbols indicate different R_i values. Lines and a small horizontal offset are added to the symbol locations to improve clarity.

the sampling matrix, but did not affect the number of full-rank cases for the conditions considered.

When extra samples are available (i.e., $R_s > R$), in principle, they are redundant and are not required for reconstruction if the sampling matrix is already full rank; however, since most measurements have noise or intrinsic variability, the extra samples can be exploited to reduce the effects of noise by including them in the linear system solution when computing \mathbf{a} . This is equivalent to using a pseudoinverse.

In the full-rank case, the extra samples do not affect the signal reconstruction but tend to reduce the effects of sampling noise and improve the system condition number. However, when the sampling matrix is not full rank when $R_s = R$, including extra samples (i.e., $R_s > R$) can result in a full-rank matrix. This is evident in Fig. 3, which compares different values of $R_i = R_s - R$. Note that the percentage of full-rank cases increases with increasing R_i .

E. Sampling Noise

We briefly consider the effects of noise. From a reconstruction point of view, noise within the signal bandwidth included in the signal *prior* to sampling is treated as part of the signal. For such band-limited noise, the reconstruction does not affect the signal-to-noise ratio.

Noise (called “sampling noise”) added to the sample values as part of the sampling process or after sampling can affect the signal-to-noise ratio of the reconstructed signal. An example of sampling noise is the quantization error resulting from analog-to-digital conversion of the signal being sampled. Such quantization error is often modeled as independent additive noise with a white spectrum [16]. Another example of sampling noise arises in microwave remote sensing, where the signal is a spatially dependent variable such as the surface brightness temperature or the normalized radar cross section. When observed by a satellite sensor, the measurements are contaminated by thermal noise from the receiver [17], which has the effect of adding white noise to the measured value after spatial sampling by

the antenna pattern and scanning geometry. Microwave sensors often use square-law detectors, which have the effect partially correlating the signal and noise and altering the noise probability distribution. For example, radiometer measurements have gamma—or chi-squared-like—distributions [17].

For simplicity, in this paper, we consider only additive noise that is independent of the signal. The measurement noise equation is [see (13) and (22)]

$$\mathbf{f}'_s = \mathbf{f}_s + \eta_s = \mathcal{D}_v \mathbf{a} + \eta_s \quad (39)$$

where \mathbf{f}'_s is the vector of noisy observations of the signal samples \mathbf{f}_s , and η_s is the vector of noise added to the signal samples. Typically, the elements of η_s are independent identically distributed (i.i.d.), although this is not required in the analysis that follows.

Given the noisy observations, the estimated sample vector $\hat{\mathbf{a}}$ is

$$\hat{\mathbf{a}} = \mathcal{D}_\Delta^{-1} (\mathbf{f}'_s + \eta_s) = \mathbf{a} + \mathcal{D}_\Delta^{-1} \eta_s = \mathbf{a} + \mathbf{a}_\eta \quad (40)$$

where $\mathbf{a}_\eta = \mathcal{D}_\Delta^{-1} \eta_s$ is the noise with the inverse sampling filter applied. The reconstructed signal thus includes an additive term consisting of the noise filtered by the reconstruction matrix, i.e.,

$$\hat{\mathbf{f}} = \mathcal{D} \mathbf{a}' + \mathcal{D} \mathbf{a}_\eta = \mathbf{f} + \eta_D \quad (41)$$

where $\eta_D = \mathcal{D} \mathcal{D}_\Delta^{-1} \eta_s$. Due to the filtering, the noise has different spectral and correlation properties in the reconstructed signal than it started with. The precise details depend on the sample locations and the aperture functions, as well as the noise properties. Some insight can be gained by examining the case of uniform sampling. For this case, the \mathcal{D} reconstruction matrix corresponds to an ideal low-pass filter, and the added noise η_D term is the low-pass-filtered noise values, i.e., the reconstruction matrix \mathcal{D} filters out frequency components of $\mathcal{D}_\Delta^{-1} \eta_s$ that extend beyond the signal band limit. In the irregular sampling case, $\mathcal{D} \mathcal{D}_\Delta^{-1}$ is a more complicated filter that amplifies some components of the noise depending on the precise sampling and aperture functions.

For a particular sampling and set of aperture functions, the postreconstruction noise spectrum can be computed using standard spectral decomposition techniques via singular value decomposition of \mathcal{D}_Δ [22]. Noise spectral components (eigenvectors) associated with small singular values of \mathcal{D}_Δ are amplified, but any noise components outside of the signal band limit defined by \mathcal{D} are eliminated. As can be expected, we have found that oversampling tends to reduce noise amplification by reducing the span of the singular values.

IV. APPLICATION EXAMPLE

We now illustrate the application of the irregular reconstruction theory for a particular microwave sensor, considering both ideal and variable apertures. While the technique can be used for a variety of sensors, for this example, we consider the passive microwave radiometer known as the Special Sensor Microwave/Imager (SSM/I) [18].

Capable of measuring up to seven different channels at different combinations of frequencies and polarizations, SSM/I is designed to measure radiometric emissions from the Earth [17]. Using a rotating antenna reflector and an integrate-and-dump filter, it collects a series of measurements over a wide swath. At the surface, the 3-dB antenna footprints range from about 15 to 70 km in the cross-scan direction and from 13 to 43 km in the along-scan direction, depending on the beam and the channel. We consider only a single beam. The measurement footprints have an elliptical shape whose size and aspect angle vary with measurement location in the swath [19].

Ignoring the effects of the atmosphere, an SSM/I measurement can be modeled as the integrated product of the surface brightness and the antenna pattern where the i th measurement z_i of the brightness temperatures is the time average of the integral of the product of the surface brightness response $T_b(x, y)$ and the spatial response function (the temporally integrated antenna gain pattern) $G_i(x, y)$ at the surface for the i th measurement [18], i.e.,

$$z_i = \frac{1}{G_i} \iint T_b(x, y) G_i(x, y) dx dy \quad (42)$$

with

$$\overline{G_i} = \iint G_i(x, iy) dx dy. \quad (43)$$

The spatial response function is thus the measurement aperture function.

Given the measurements z_i , we want to estimate the surface brightness temperature T_b . To do this, following the discussion in Section I, we assume that T_b is band limited, replace the integrals with summations of the sampled signals and aperture functions, and use reconstruction techniques to recover the band-limited T_b .

To illustrate the application of reconstruction theory, a simulation of the sampling and response function for the 37-GHz H-polarization SSM/I channel is conducted. An HSI pixel spacing¹³ of 6.25 km is selected with the fine processing grid size set at $N_1 = N_2 = 100$, which corresponds to a 625 km \times 625 km area. This is approximately one half the nominal swath width, which was chosen for convenience.

Since the average spacing of the samples is approximately 25 km, we cannot expect the effective resolution of the reconstruction to provide much better resolution. Hence, we set $d_1 = d_2 = 4$ so that $M_1 = M_2 = 25$, which corresponds to a 25-km signal resolution. Note that denser sampling (more samples over the same area) can support finer product image resolution. This can be achieved by combining multiple satellite passes over the target area [20].

The measurement response is modeled as an elliptical Gaussian function with one-half power dimensions of 37.5 km \times 25 km. These are the measurement apertures. The ellipse aspect angle relative to the image grid is determined by the antenna scan angle, which varies across the swath. Fig. 4(a) illustrates

the measurement locations. Note that the measurements locations form an irregular sampling grid. Fig. 4(b) shows a few of the aperture functions, which vary over the swath, resulting in spatially varying spatial response functions. The major axis of the aperture is aligned with the grid near the bottom, but is rotated by 60° near the top.

For the simulation, a synthetic “truth” image is constructed at fine grid resolution, as shown in Fig. 4(d), that contains various features, including “spots” of varying sizes and image gradients. The span of T_b values is realistic for land imaging for the 37H SSM/I channel [19]. The truth image is ideally low-pass filtered to band limit it to 25-km resolution, as shown in Fig. 4(e). This image represents the best that can be recovered from the truth image in a $M_1 \times M_2$ band-limited sense. The mottling and feature smoothing in the image are the result of the ideal band limiting. The root-mean-square (rms) difference between the band-limited and non-band-limited truth images is 4.80 K.

The various sampling and reconstruction matrices are numerically computed. The true \mathbf{a} is computed using a 2-D fast Fourier transform. The \mathcal{D} matrix is independent of the measurement locations and depends only on M_1 , M_2 , N_1 , and N_2 . Using the sampling locations in Fig. 4(a), the \mathcal{D}_Δ matrix is computed. The \mathcal{D}_v matrix is computed using the measurement-varying aperture function and the measurement location. In this case, there are $R = R_s = 625$ measurements. The \mathcal{D}_v matrix is full rank.

Simulated noise-free measurements with ideal apertures are created along with simulated measurements for realistic spatially varying apertures using (31) and (36), respectively. Noisy measurements are simulated by adding unit variance i.i.d. Gaussian noise to the simulated noise-free measurements.

Because \mathcal{D}_Δ and \mathcal{D}_v are full rank, the reconstruction from the noise-free measurements is exact to within numerical precision, i.e., both the ideal and realistic aperture reconstructions are the same as the true band-limited image in Fig. 4(e). In these numerical experiments, the condition numbers for the ideal and realistic aperture cases are 20 and 1982, which results in linear systems that are readily solvable with standard software.

Referring to (41), the noisy measurements are the sum of a noise term and the reconstructed signal. The noise terms for the same particular realization of the noise for the ideal and realistic apertures are shown in Fig. 4(g) and (h). We observe that the unit variance additive noise has been significantly enhanced, particularly for the aperture case, where the reconstruction filter applied to the noise has created a diagonal ripple. It is thus apparent that, for this particular problem, while the signal reconstruction is exact, the reconstruction of noisy measurements is sensitive to the noise level.

In conventional SSM/I data processing, the measurements are often gridded onto a 25-km grid $N'_1 = N'_2 = 25$ using a “drop-in-the-bucket” (DIB) technique where, for each DIB grid element, all of the measurements whose centers fall within the grid element are averaged into the value reported by that pixel. The DIB resolution is limited to the sum of the grid size and the measurement response dimensions, in this case, about 50 km or about twice as coarse as the reconstruction grid. The number of measurements falling within each DIB

¹³The pixel spacing is the same as the “posting resolution” or spacing of the reconstructed signal.

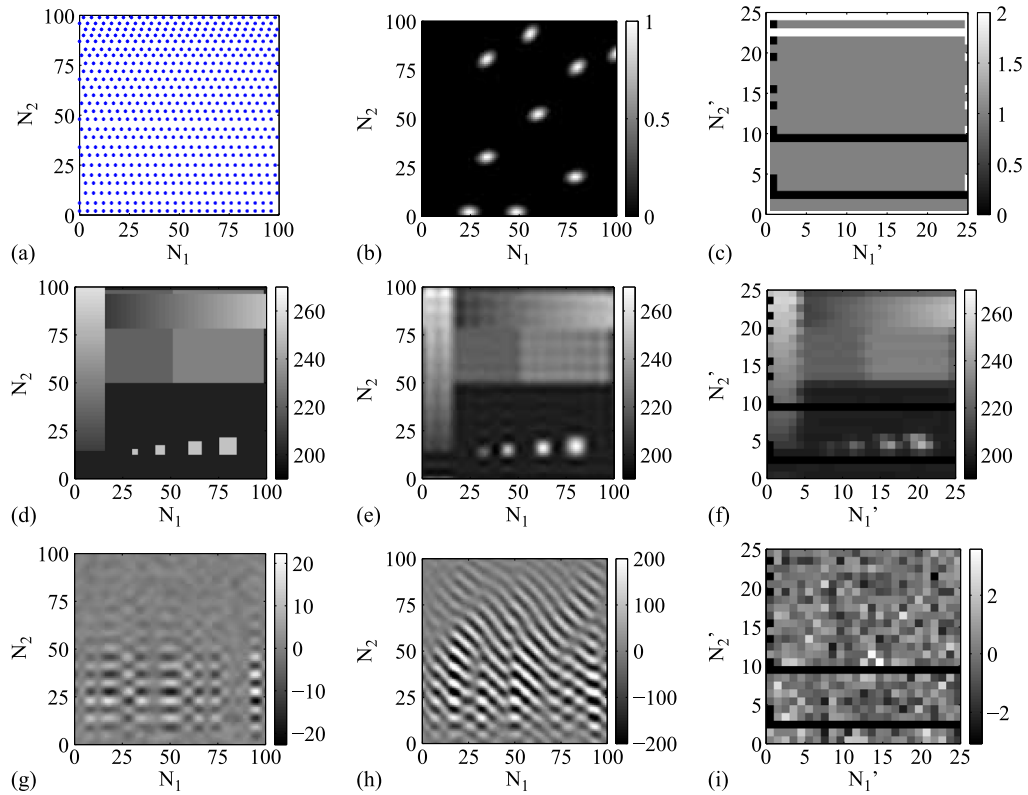


Fig. 4. Illustrative results from an SSM/I measurement and reconstruction simulation. (a) Measurement locations. Underlying pixel spacing is 6.25 km. (b) Examples of the spatial measurement response function (aperture) at several locations. (c) Count of the number of measurements in each 25-km grid element. (d) Synthetic “truth” image (not band limited). (e) Band-limited “truth” image. Band limit is at 25 km. (f) DIB image. (g) Reconstructed noise without aperture. (h) Reconstructed noise with aperture. (i) DIB noise example. Horizontal bands in lower portion of (c), (f), and (i) are DIB grid pixels containing no measurements—see text.

TABLE I
SUMMARY OF SSM/I SIMULATION RMS DIFFERENCE STATISTICS.
THE RMS DIFFERENCE BETWEEN THE BAND-LIMITED AND
NON-BAND-LIMITED TRUTH IMAGES IS 4.80 K

| Case | Band-limited Truth | Non-band-limited Truth | Noise Term |
|--------------------|-----------------------|---------------------------|---------------|
| Antenna Aperture | 0.00 | 4.80 | 51.8 |
| Ideal Aperture | 0.00 | 4.80 | 2.65 |
| Drop-in-the-Bucket | 6.60 | 8.00 | 0.95 |

grid element is shown in Fig. 4(c). Note that the number of measurements falling within a DIB grid element varies over the area and that some grid elements contain no measurements at all, resulting in gaps in the image, which are rows in this case. These gaps can be eliminated by increasing the grid size, which further lowers the image resolution. The DIB image estimate is shown in Fig. 4(f). Note the reduced effective resolution of the DIB image compared with the reconstructed image, as well as the coarser features. Grid elements with no measurements are shown in dark blue. The DIB noise term is shown in Fig. 4(i).

A comparison of the rms errors for each image formation case is given in Table I. Comparing the DIB, the reconstructed images, and the rms difference statistics, the improved accuracy and resolution of the reconstruction are apparent. However, the DIB noise level is also much smaller than the reconstructed case; thus, there is a tradeoff between resolution and noise level. This tradeoff can be exploited more finely using

partial reconstruction techniques such as discussed in [13] and [20]. Whether a particular application can tolerate the higher noise level in exchange for finer effective resolution is application specific.

V. CONCLUSION

This paper has discussed the theory of signal reconstruction from irregularly sampled data with variable apertures where different measurements may have different aperture functions. This situation is common in microwave sensors where the observations have irregular spacing and different antenna gain patterns resulting in different measurement functions for different measurements.

The reconstruction methods presented in this paper can be used for both real and complex signals. In either case, the various D and \mathcal{D} matrices are real.

We have focused on exact band-limited reconstruction of a band-limited discrete signal. For the 1-D case, so long as there are a sufficient number of distinct samples and the aperture function is reasonably well behaved, a band-limited periodic signal can be exactly reconstructed. In the 2-D case, the situation is more complicated, since not all sampling configurations can support full signal reconstruction. However, so long as the variable aperture function sampling matrix $[\mathbf{D}_v$ or $\mathcal{D}_v]$ is full column rank, a band-limited periodic function can be exactly

reconstructed, within the limits of numerical precision, by inverting a linear system. When the samples have added noise, the sampling noise is filtered by the reconstruction matrix, which can enhance the impact of the noise. Example results are provided using a simulation-based realistic satellite sensor, i.e., the SSM/I microwave radiometer.

A number of illustrative numerical examples that demonstrate 1-D and 2-D irregular and variable aperture reconstruction are provided at www.mers.byu.edu/reconstruction. MATLAB source code is included to illustrate the various reconstruction algorithms discussed. Links to other software cited in this paper are provided on this same site.

We note that alternative reconstruction methods have been developed for the case when the signal is not band limited or when only approximate or partially reconstructed results are needed, e.g., [2]–[4], [12] and [13], and [20] and [21]. These may be numerically more efficient than the exact method considered here. Inexact methods that incorporate the noise statistics using Wiener–Kolmogorov smoothing to minimize the total error are also available, e.g., [22].

APPENDIX

A. Invertability of \mathbf{D}_\circ

For the regular sampling case with $R = 2M + 1$, the matrix \mathbf{D}_\circ defined in (12) can be written as the product of two matrices, i.e., $\mathbf{D}_\circ = \mathbf{BC}$, where

$$\mathbf{B} = \begin{bmatrix} W_N^{-Mn_0} & \dots & W_N^{Mn_0} \\ \vdots & \ddots & \vdots \\ W_N^{-Mn_{2M}} & \dots & W_N^{Mn_{2M}} \end{bmatrix} \quad (44)$$

$$\mathbf{C} = \begin{bmatrix} 1 & W_N^{Md} & \dots & W_N^{M2Md} \\ \vdots & \vdots & \ddots & \vdots \\ 1 & W_N^{-Md} & \dots & W_N^{-M2Md} \end{bmatrix}. \quad (45)$$

Letting $W_N^{n_j} = b_j, j = 0, 1, \dots, 2M$, then $W_N^{n_{j^l}} = b_j^l$ and the matrix \mathbf{B} can be written as

$$\mathbf{B} = \begin{bmatrix} b_0^{-M} & \dots & b_0^{-1} & 1 & b_0 & \dots & b_0^M \\ \vdots & & \vdots & \vdots & \vdots & & \vdots \\ b_{2M}^{-M} & \dots & b_{2M}^{-1} & 1 & b_{2M} & \dots & b_{2M}^M \end{bmatrix}. \quad (46)$$

We note that \mathbf{B} is a Vandermonde matrix with complex entries b_i , where $b_i \neq b_j \forall i \neq j, j = 0, 1, \dots, 2M$. It is well known that the inverse of a Vandermonde matrix exists¹⁴; therefore, \mathbf{B}^{-1} exists.

¹⁴In fact, a closed-form analytic inverse of a general Vandermonde matrix has been developed [23].

Similarly, letting $W_N^{-(M+k)d} = c_k, k = 0, 1, \dots, 2M$, then $W_N^{-(M+k)pd} = c_k^j$, and matrix \mathbf{C} is

$$\mathbf{C} = \begin{bmatrix} 1 & c_0 & c_0^2 & \dots & c_0^{2M} \\ \vdots & \vdots & \vdots & & \vdots \\ 1 & c_{2M} & c_{2M}^2 & \dots & c_{2M}^{2M} \end{bmatrix} \quad (47)$$

which is also a Vandermonde matrix with $c_i \neq c_j$ for $i \neq j$; therefore, \mathbf{C}^{-1} always exists. Since \mathbf{B}^{-1} and \mathbf{C}^{-1} exist, and recalling that $\mathbf{D}_\circ = \mathbf{BC}$, it follows that $\mathbf{D}_\circ^{-1} = \mathbf{C}^{-1}\mathbf{B}^{-1}$ exists.

B. Invertability of \mathbf{D}_Δ

The matrix \mathbf{D}_Δ defined in (14) can be factored as the product of two matrices, i.e., $\mathbf{D}_\Delta = \mathbf{BC}$, where

$$\mathbf{B} = \begin{bmatrix} W_N^{-Mn_1} & \dots & W_N^{Mn_1} \\ \vdots & \ddots & \vdots \\ W_N^{-Mn_R} & \dots & W_N^{Mn_R} \end{bmatrix} \quad (48)$$

and \mathbf{C} is precisely the same matrix as in the regular case [see (47)]. Note that \mathbf{C} is not dependent on the n_j values. Using $b_j = W_N^{n_j-1}$, \mathbf{B} can be written as

$$\mathbf{B} = \begin{bmatrix} b_0^{-M} & \dots & b_0^{-1} & 1 & b_0 & \dots & b_0^M \\ \vdots & & \vdots & \vdots & \vdots & & \vdots \\ b_{2M}^{-M} & \dots & b_{2M}^{-1} & 1 & b_{2M} & \dots & b_{2M}^M \end{bmatrix}. \quad (49)$$

To see that \mathbf{B} is invertable for any disjoint set of n_j values, note that the matrix \mathbf{B} can be factored into the product of two matrices, i.e., $\mathbf{B} = \mathbf{AV}$, where

$$\mathbf{A} = \begin{bmatrix} W_N^{-Mn_0} & 0 & 0 \\ \vdots & \ddots & \vdots \\ 0 & 0 & W_N^{Mn_0} \end{bmatrix} \quad (50)$$

$$\mathbf{V} = \begin{bmatrix} 1 & W_N^{n_0} & \dots & W_N^{2Mn_0} \\ \vdots & \vdots & \ddots & \vdots \\ 1 & W_N^{n_{2M}} & \dots & W_N^{2Mn_{2M}} \end{bmatrix}. \quad (51)$$

\mathbf{A} is a diagonal matrix with nonzero diagonal elements; therefore, \mathbf{A}^{-1} exists. Letting $v_k = W_N^{n_{k-1}}$, \mathbf{V} can be written as

$$\mathbf{V} = \begin{bmatrix} 1 & v_0 & v_0^2 & \dots & v_0^{2M} \\ \vdots & \vdots & \vdots & & \vdots \\ 1 & v_{2M} & v_{2M}^2 & \dots & v_{2M}^{2M} \end{bmatrix} \quad (52)$$

which is a Vandermonde matrix with $v_i \neq v_j \forall i \neq j$; therefore, \mathbf{V}^{-1} exists. Given that $\mathbf{A}^{-1}, \mathbf{V}^{-1}$, and \mathbf{C}^{-1} exist and $\mathbf{D}_\Delta = \mathbf{BC} = \mathbf{AVC}$, it follows that $\mathbf{D}_\Delta^{-1} = \mathbf{C}^{-1}\mathbf{V}^{-1}\mathbf{A}^{-1}$ exists for any disjoint set of n_j .

ACKNOWLEDGMENT

The authors would like to thank the anonymous reviewers for their suggestions on the draft of this paper.

REFERENCES

- [1] A. V. Oppenheim and A. S. Willsky, *Signals and Systems*. Englewood Cliffs, NJ, USA: Prentice-Hall, 1983.
- [2] M. Unser, "Sampling—50 years after Shannon," *Proc. IEEE*, vol. 88, no. 4, pp. 569–587, Apr. 2000.
- [3] M. Migliaccio and F. Bruno, "A new interpolation kernel for SAR interferometric registration," *IEEE Trans. Geosci. Remote Sens.*, vol. 41, no. 5, pp. 1105–1110, May 2003.
- [4] M. Migliaccio, F. Nunziata, F. Bruno, and F. Casu, "Knab sampling window for InSAR data interpolation," *IEEE Geosci. Remote Sens. Lett.*, vol. 4, no. 3, pp. 397–400, Jul. 2007.
- [5] H. Feichtinger and K. Gröchenig, "Iterative reconstruction of multivariate band-limited function from irregular sampling values," *SIAM J. Math. Anal.*, vol. 23, no. 1, pp. 244–261, Jan. 1992.
- [6] H. G. Feichtinger, K. Gröchenig, and T. Strohmer, "Efficient numerical methods in non-uniform sampling theory," *Numer. Math.*, vol. 69, pp. 423–440, Feb. 1995.
- [7] K. Gröchenig, "Reconstruction algorithms in irregular sampling," *Math. Comput.*, vol. 59, no. 199, pp. 181–194, Jul. 1992.
- [8] K. Gröchenig, "A discrete theory of irregular sampling," *Linear Algebra Appl.*, vol. 193, pp. 129–150, Nov. 1993.
- [9] X. Xu, W. Ye, and A. Entezari, "Bandlimited reconstruction of multidimensional images from irregular samples," *IEEE Trans. Image Process.*, vol. 22, no. 10, pp. 3950–3960, Oct. 2013.
- [10] B. A. Williams and D. G. Long, "Reconstruction from aperture-filtered samples with application to scatterometer image reconstruction," *IEEE Trans. Geosci. Remote Sens.*, vol. 49, no. 5, pp. 1663–1676, May 2011.
- [11] W. Sun and X. Zhou, "Reconstruction of band-limited signals from local averages," *IEEE Trans. Inf. Theory*, vol. 48, no. 11, pp. 2955–2963, Nov. 2002.
- [12] Y. Censor, "Finite series-expansion reconstruction methods," *Proc. IEEE*, vol. 71, no. 3, pp. 409–419, Mar. 1983.
- [13] D. S. Early and D. G. Long, "Image reconstruction and enhanced resolution imaging from irregular samples," *IEEE Trans. Geosci. Remote Sens.*, vol. 39, no. 2, pp. 291–302, Feb. 2001.
- [14] F. Lenti, F. Nunziata, C. Estatico, and M. Migliaccio, "On the spatial resolution enhancement of microwave radiometer data in banach spaces," *IEEE Trans. Geosci. Remote Sens.*, vol. 52, no. 3, pp. 1834–1842, Mar. 2014.
- [15] H. R. Künsch, E. Agrell, and F. A. Hamprecht, "Optimal lattices for sampling," *IEEE Trans. Inf. Theory*, vol. 51, no. 2, pp. 634–647, Feb. 2005.
- [16] A. V. Oppenheim and R. W. Schaffer, *Discrete-Time Signal Processing*. Upper Saddle River, NJ, USA: Prentice-Hall, 2010.
- [17] F. T. Ulaby and D. G. Long, *Microwave Radar and Radiometric Remote Sensing*. Ann Arbor, MI, USA: Univ. Michigan Press, 2014.
- [18] J. P. Hollinger, J. L. Pierce, and G. A. Poe, "SSM/I instrument evaluation," *IEEE Trans. Geosci. Remote Sens.*, vol. 28, no. 5, pp. 781–790, Sep. 1990.
- [19] D. G. Long and D. L. Daum, "Spatial resolution enhancement of SSM/I data," *IEEE Trans. Geosci. Remote Sens.*, vol. 36, no. 2, pp. 407–417, Mar. 1998.
- [20] D. G. Long and M. J. Brodzik, "Optimum image formation for spaceborne microwave radiometer products," *IEEE Trans. Geosci. Remote Sens.*, vol. 54, no. 5, pp. 2763–2779, May 2016.
- [21] P. L. Butzer and J. Lei, "Approximation of signals using measured sampled values and error analysis," *Commun. Appl. Anal.*, vol. 4, no. 2, pp. 245–255, Jan. 2000.
- [22] M. Foster, "An application of the Wiener–Kolmogorov smoothing theory to matrix inversion," *J. Soc. Ind. Appl. Math.*, vol. 9, no. 3, pp. 387–392, Sep. 1961.
- [23] M. E. A. El-Mikkawy, "Explicit inverse of a generalized Vandermonde matrix," *Appl. Math. Comput.*, vol. 146, no. 2/3, pp. 643–651, Dec. 2003.



David G. Long (S'80–SM'98–F'08) received the Ph.D. degree in electrical engineering from the University of Southern California, Los Angeles, CA, USA, in 1989.

From 1983 to 1990, he was with the NASA Jet Propulsion Laboratory (JPL), where he developed advanced radar remote sensing systems. While at JPL, he was the Project Engineer on the NASA Scatterometer (NSCAT) project, which flew from 1996 to 1997. He also managed the SCANSAT project, the precursor to SeaWinds, which was flown in 1999 on QuikSCAT, in 2002 on ADEOS-II, and in 2014 on the International Space Station. He is currently a Professor with the Electrical and Computer Engineering Department, Brigham Young University (BYU), Provo, UT, USA, where he teaches upper division and graduate courses in communications, microwave remote sensing, radar, and signal processing and is the Director of the BYU Center for Remote Sensing. He is the Principal Investigator on several NASA-sponsored research projects in remote sensing. He has over 400 publications in various areas, including signal processing, radar scatterometry, and synthetic aperture radar. His research interests include microwave remote sensing, radar theory, space-based sensing, estimation theory, signal processing, and mesoscale atmospheric dynamics.

Prof. Long is an Associate Editor of the IEEE GEOSCIENCE AND REMOTE SENSING LETTERS. He has been a recipient of the NASA Certificate of Recognition several times.



Reinhard O. W. Franz received the Ph.D. degree in mathematics from Bielefeld University, Bielefeld, Germany, in 1988.

Since 1993, he has been teaching mathematics courses at Brigham Young University, Provo, UT, USA. His research interests include topological algebra, nonstandard analysis, combinatorics (periodic tilings, meanders, etc.), and signal reconstruction problems.